

Lepton Flavour Violation in SUSY-seesaw: an update

Ernesto Arganda^a and María J. Herrero^b

Departamento de Física Teórica and Instituto de Física Teórica, IFT-UAM/CSIC,
Universidad Autónoma de Madrid, Cantoblanco, E-28049 Madrid, Spain

Abstract. Here we update the predictions for lepton flavour violating tau and muon decays, $l_j \rightarrow l_i \gamma$, $l_j \rightarrow 3l_i$, and $\mu - e$ conversion in nuclei. We work within a SUSY-seesaw context where the particle content of the Minimal Supersymmetric Standard Model is extended by three right handed neutrinos plus their corresponding SUSY partners, and where a seesaw mechanism for neutrino mass generation is implemented. Two different scenarios with either universal or non-universal soft supersymmetry breaking Higgs masses at the gauge coupling unification scale are considered. After comparing the predictions with present experimental bounds and future sensitivities, the most promising processes are particularly emphasised.

PACS. 11.30.Hv Flavor symmetries – 12.60.Jv SUSY models – 14.60.St Right-handed neutrinos

1 LFV within the SUSY Seesaw

The current knowlegde of neutrino mass differences and mixing angles clearly indicates that lepton flavour number is not a conserved quantum number in Nature. However, the lepton flavour violation (LFV) has so far been observed only in the neutrino sector. One challenging task for the present and future experiments will then be to test if there is or there is not LFV in the charged lepton sector as well.

Here we focus in the Minimal Supersymmetric Standard Model (MSSM) enlarged by three right handed neutrinos and their SUSY partners where potentially observable LFV effects in the charge lepton sector are expected to occur. We further assume a seesaw mechanism for neutrino mass generation and use, in particular, the parameterisation proposed in [1] where the solution to the seesaw equation is written as $m_D = Y_\nu v_2 = \sqrt{m_N^{\text{diag}}} R \sqrt{m_\nu^{\text{diag}}} U_{\text{MNS}}^\dagger$. Here, R is defined by θ_i ($i = 1, 2, 3$); $v_{1(2)} = v \cos(\sin)\beta$, $v = 174$ GeV; $m_\nu^{\text{diag}} = \text{diag}(m_{\nu_1}, m_{\nu_2}, m_{\nu_3})$ denotes the three light neutrino masses, and $m_N^{\text{diag}} = \text{diag}(m_{N_1}, m_{N_2}, m_{N_3})$ the three heavy ones. U_{MNS} is given by the three (light) neutrino mixing angles θ_{12}, θ_{23} and θ_{13} , and three phases, δ, ϕ_1 and ϕ_2 . With this parameterisation is easy to accommodate the neutrino data, while leaving room for extra neutrino mixings (from the right handed sector). It further allows for large Yukawa couplings $Y_\nu \sim \mathcal{O}(1)$ by choosing large entries in m_N^{diag} and/or θ_i .

The particular LFV processes here studied are shown in table 1, together with their present experimental bounds and future planned sensitivities. The

predictions in the following are for two different constrained MSSM-seesaw scenarios, with universal and non-universal Higgs soft masses and with respective parameters (in addition to the previous neutrino sector parameters): 1) CMSSM-seesaw: $M_0, M_{1/2}, A_0 \tan \beta$, and $\text{sign}(\mu)$, and 2) NUHM-seesaw: $M_0, M_{1/2}, A_0 \tan \beta$, $\text{sign}(\mu)$, $M_{H_1} = M_0(1 + \delta_1)^{1/2}$ and $M_{H_2} = M_0(1 + \delta_2)^{1/2}$. All the predictions presented here include the full set of SUSY one-loop contributing diagrams, mediated by γ, Z , and Higgs bosons, as well as boxes, and do not use the Leading Logarithmic (LLog) nor the mass insertion approximations. This is a very short summary of the works in Refs. [2], [3] and [4] to which we refer the reader for more details.

Table 1. Present bounds and future sensitivities for the LFV processes.

LFV process	Present bound	Future sensitivity
BR($\mu \rightarrow e \gamma$)	1.2×10^{-11}	1.3×10^{-13}
BR($\tau \rightarrow e \gamma$)	1.1×10^{-7}	10^{-8}
BR($\tau \rightarrow \mu \gamma$)	4.5×10^{-8}	10^{-8}
BR($\mu \rightarrow 3e$)	1.0×10^{-12}	10^{-13}
BR($\tau \rightarrow 3e$)	2.0×10^{-7}	10^{-8}
BR($\tau \rightarrow 3\mu$)	1.9×10^{-7}	10^{-8}
CR($\mu - e$, Ti)	4.3×10^{-12}	10^{-18}
CR($\mu - e$, Au)	7×10^{-13}	-

2 Results and Discussion

We focus on the dependence on the most relevant parameters which, for the case of hierarchical (degenerate) heavy neutrinos, are: the neutrino mass m_{N_3}

^a Email: ernesto.arganda@uam.es

^b Email: Talk given by maria.herrero@uam.es

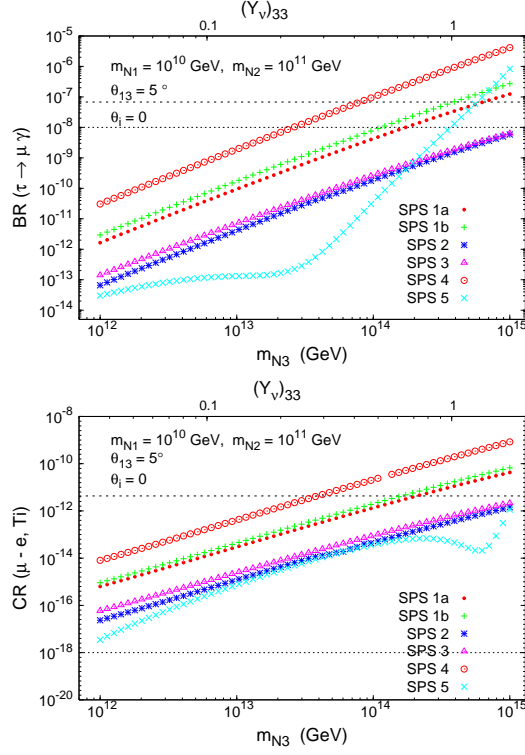


Fig. 1. $\tau \rightarrow \mu\gamma$ and $\text{CR}(\mu \rightarrow e, \text{Ti})$ as a function of m_{N_3} . The predictions for SPS 1a (dots), 1b (crosses), 2 (asterisks), 3 (triangles), 4 (circles) and 5 (times) are included. On the upper horizontal axis we display the associated value of $(Y_\nu)_{33}$. In each case, we set $\theta_{13} = 5^\circ$, and $\theta_i = 0$. The upper (lower) horizontal line denotes the present experimental bound (future sensitivity).

(m_N) , $\tan\beta$, θ_1 and θ_2 . We also study the sensitivity of the BRs to θ_{13} . The other input seesaw parameters m_{N_1} , m_{N_2} and θ_3 , play a secondary role since the BRs do not strongly depend on them. The light neutrino parameters are fixed to: $m_{\nu_2}^2 = \Delta m_{\text{sol}}^2 + m_{\nu_1}^2$, $m_{\nu_3}^2 = \Delta m_{\text{atm}}^2 + m_{\nu_1}^2$, $\Delta m_{\text{sol}}^2 = 8 \times 10^{-5} \text{ eV}^2$, $\Delta m_{\text{atm}}^2 = 2.5 \times 10^{-3} \text{ eV}^2$, $m_{\nu_1} = 10^{-3} \text{ eV}$, $\theta_{12} = 30^\circ$, $\theta_{23} = 45^\circ$, $\theta_{13} \lesssim 10^\circ$ and $\delta = \phi_1 = \phi_2 = 0$.

The results for the CMSSM-seesaw scenario are collected in Figs. 1 through 5. In Fig. 1, we display the predictions of $\text{BR}(\tau \rightarrow \mu\gamma)$ and $\text{CR}(\mu \rightarrow e, \text{Ti})$ as a function of the heaviest neutrino mass m_{N_3} for the various SPS points [5], and for the particular choice $\theta_i = 0$ ($i = 1, 2, 3$) and $\theta_{13} = 5^\circ$. We have also considered the case of degenerate heavy neutrino spectra (not shown here). In both scenarios for degenerate and hierarchical heavy neutrinos, we find a strong dependence on the heavy neutrino masses, with the expected behaviour $|m_N \log m_N|^2$ of the LLog approximation, except for SPS 5 point, which fails by a factor of $\sim 10^4$. The rates for the various SPS points exhibit the following hierarchy, $\text{BR}_4 > \text{BR}_{1b} \gtrsim \text{BR}_{1a} > \text{BR}_3 \gtrsim \text{BR}_2 > \text{BR}_5$. This behaviour can be understood in terms of the growth of the BRs with $\tan\beta$, and from the different mass spectra associated with each point. Most of the studied processes reach their experimental limit at $m_{N_3} \in$

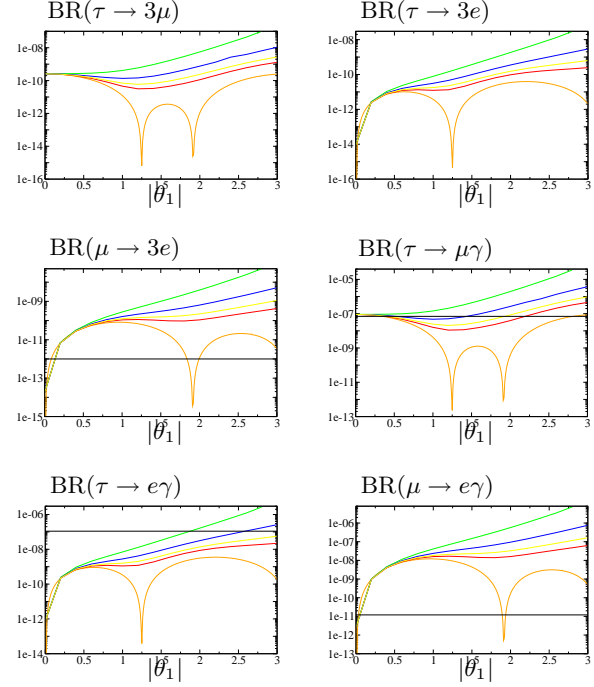


Fig. 2. Dependence of LFV τ and μ decays with $|\theta_1|$ for SPS 4 case with $\arg(\theta_1) = 0, \pi/10, \pi/8, \pi/6, \pi/4$ in radians (lower to upper lines), $(m_{N_1}, m_{N_2}, m_{N_3}) = (10^8, 2 \times 10^8, 10^{14})$ GeV, $\theta_2 = \theta_3 = 0$, $\theta_{13} = 0$ and $m_{\nu_1} = 0$. The horizontal lines are the present experimental bounds.

$[10^{13}, 10^{15}]$ which corresponds to $Y_\nu^{33,32} \sim 0.1 - 1$. At present, the most restrictive one is $\mu \rightarrow e\gamma$ (which sets bounds for SPS 1a of $m_{N_3} < 10^{13} - 10^{14}$ GeV), although $\mu - e$ conversion will be the best one in future, with a sensitivity to $m_{N_3} > 10^{12}$ GeV.

Fig. 2 shows the behaviour of the six considered LFV τ and μ decays, for SPS 4 point, as a function of $|\theta_1|$, for various values of $\arg\theta_1$. We see clearly that the BRs for $0 < |\theta_1| < \pi$ and $0 < \arg\theta_1 < \pi/2$ can increase up to a factor $10^2 - 10^4$ with respect to $\theta_i = 0$. Similar results have been found for θ_2 , while BRs are nearly constant with θ_3 in the case of hierarchical neutrinos. The behaviour of $\text{CR}(\mu \rightarrow e, \text{Ti})$ with θ_i is very similar to that of $\text{BR}(\mu \rightarrow e\gamma)$ and $\text{BR}(\mu \rightarrow 3e)$. For instance, Fig. 3 shows the dependence of $\text{CR}(\mu \rightarrow e, \text{Ti})$ with θ_2 , and illustrates that for large θ_2 , rates up to a factor $\sim 10^4$ larger than in the $\theta_i = 0$ case can be obtained.

In Fig. 4 we show the dependence of $\mu \rightarrow e\gamma$, $\mu \rightarrow 3e$ and $\mu - e$ conversion on the light neutrino mixing angle θ_{13} . These figures clearly manifest the very strong sensitivity of their rates to the θ_{13} mixing angle for hierarchical heavy neutrinos. Indeed, varying θ_{13} from 0 to 10° leads to an increase in the rates by as much as five orders of magnitude. On the other hand, since $\mu \rightarrow e\gamma$ is very sensitive to θ_{13} , but $\text{BR}(\tau \rightarrow \mu\gamma)$ is clearly not, and since both BRs display the same approximate behaviour with m_{N_3} and $\tan\beta$, one can study the impact that a potential future measurement of θ_{13} and these two rates can have on the knowledge of the otherwise unreachable heavy neutrino parameters. The correlation of these two observables as a

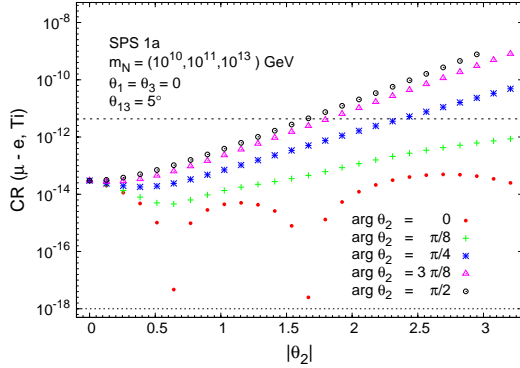


Fig. 3. $\text{CR}(\mu - e, \text{Ti})$ as a function of $|\theta_2|$, for SPS 1a case with $\arg \theta_2 = \{0, \pi/8, \pi/4, 3\pi/8, \pi/2\}$ (dots, crosses, asterisks, triangles and circles, respectively), $m_{N_i} = (10^{10}, 10^{11}, 10^{13})$ GeV, $\theta_{13} = 5^\circ$. The upper (lower) horizontal line denotes the present experimental bound (future sensitivity).

function of m_{N_3} , is shown in Fig. 5 for SPS 1a. Comparing these predictions for the shaded areas along the expected diagonal “corridor”, with the allowed experimental region, allows to conclude about the impact of a θ_{13} measurement on the allowed/excluded m_{N_3} values. The most important conclusion from Fig. 5 is that for SPS 1a, and for the parameter space defined in the caption, an hypothetical θ_{13} measurement larger than 1° , together with the present experimental bound on the $\text{BR}(\mu \rightarrow e\gamma)$, will have the impact of excluding values of $m_{N_3} \gtrsim 10^{14}$ GeV. Moreover, with the planned MEG sensitivity, the same θ_{13} measurement could further exclude $m_{N_3} \gtrsim 3 \times 10^{12}$ GeV.

The numerical results for the NUHM-seesaw scenario as a function of $M_0 = M_{1/2} = M_{\text{SUSY}}$ are collected in Figs. 6 through 8. The behaviour of the predicted m_{H^0} as a function of M_{SUSY} is shown in Fig. 6. The most interesting solutions with important phenomenological implications are found for negative δ_1 and positive δ_2 . Notice that, for all the explored $\delta_{1,2}$ values, we find a value of m_{H^0} that is significantly smaller than in the universal case ($\delta_{1,2} = 0$).

In Fig. 7 the various contributions from the γ -, Z -, Higgs mediated penguins and box diagrams as a function of M_{SUSY} are shown. Here, we choose $\delta_1 = -1.8$ and $\delta_2 = 0$. We observe a very distinct behaviour with M_{SUSY} of the Higgs-mediated contributions compared to those of the CMSSM case. In fact, the Higgs-mediated contribution can equal, or even exceed that of the photon, dominating the total conversion rate in the large $M_0 = M_{1/2}$ region. These larger Higgs contributions are the consequence of their exclusive SUSY non-decoupling behaviour for large M_{SUSY} , and of the lighter Higgs boson mass values encountered in this region, as previously illustrated in Fig. 6.

In Fig. 8 we display the predicted $\mu - e$ conversion rates for other nuclei, concretely Al, Ti, Sr, Sb, Au and Pb, as a function of M_{SUSY} . We clearly see that $\text{CR}(\mu - e, \text{Sb}) > \text{CR}(\mu - e, \text{Sr}) > \text{CR}(\mu - e, \text{Ti}) > \text{CR}(\mu - e, \text{Au}) > \text{CR}(\mu - e, \text{Pb}) > \text{CR}(\mu - e, \text{Al})$. The

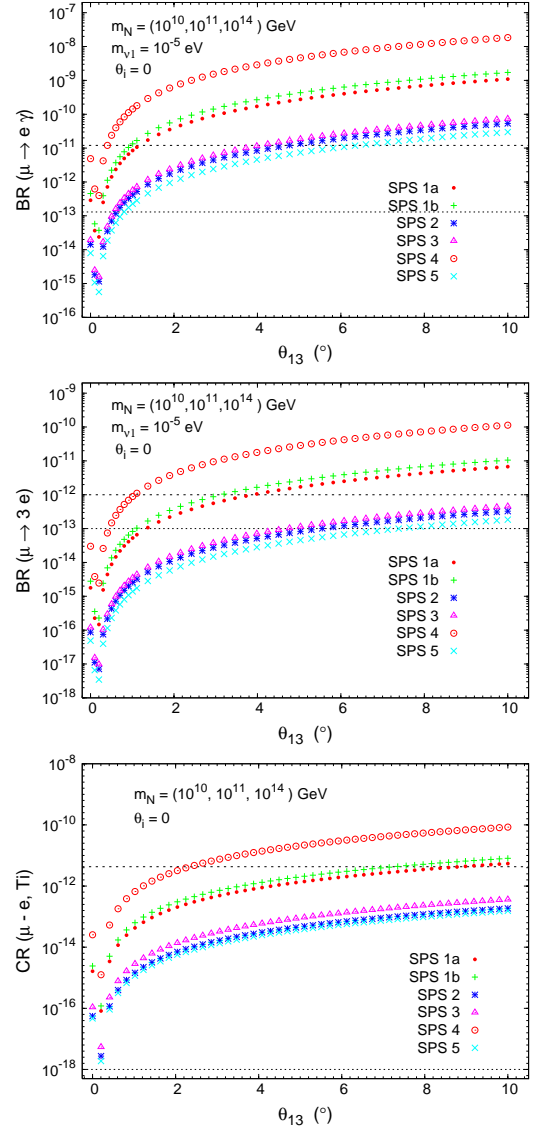


Fig. 4. $\text{BR}(\mu \rightarrow e\gamma)$, $\text{BR}(\mu \rightarrow 3e)$ and $\text{CR}(\mu - e, \text{Ti})$ as a function of θ_{13} (in degrees), for SPS 1a (dots), 1b (crosses), 2 (asterisks), 3 (triangles), 4 (circles) and 5 (times), with $\theta_i = 0$ and $m_{N_i} = (10^{10}, 10^{11}, 10^{14})$ GeV. The upper (lower) horizontal line denotes the present experimental bound (future sensitivity).

most important conclusion from Fig. 8 is that we have found predictions for Gold nuclei which, for the input parameters in this plot, are above its present experimental bound throughout the explored M_{SUSY} interval. Finally, although not shown here for shortness, we have also found an interesting loss of correlation between the predicted $\text{CR}(\mu - e, \text{Ti})$ and $\text{BR}(\mu \rightarrow e\gamma)$ in the NUHM-seesaw scenario compared to the universal case where these are known to be strongly correlated. This loss of correlation occurs when the Higgs-contributions dominate the photon-contributions and could be tested if the announced future sensitivities in these quantities are reached.

In conclusion, we believe that a joint measurement of the LFV branching ratios, the $\mu - e$ conversion rates,

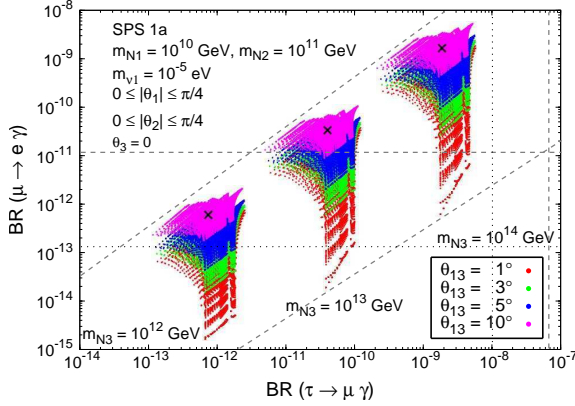


Fig. 5. Correlation between $\text{BR}(\mu \rightarrow e \gamma)$ and $\text{BR}(\tau \rightarrow \mu \gamma)$ as a function of m_{N_3} , for SPS 1a, and impact of θ_{13} . The areas displayed represent the scan over θ_i . From bottom to top, the coloured regions correspond to $\theta_{13} = 1^\circ$, 3° , 5° and 10° (red, green, blue and pink, respectively). Horizontal and vertical dashed (dotted) lines denote the experimental bounds (future sensitivities).

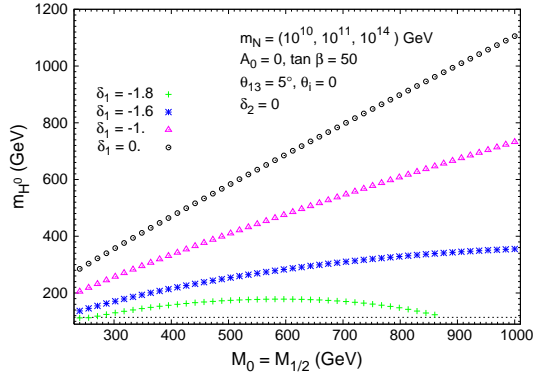


Fig. 6. Mass of m_{H^0} as a function of $M_0 = M_{1/2}$, for fixed values of $\delta_1 = \{-1.8, -1.6, -1, 0\}$ (respectively crosses, asterisks, triangles and circles), with $m_{N_i} = (10^{10}, 10^{11}, 10^{14})$ GeV, $\theta_i = 0$, $A_0 = 0$, $\tan \beta = 50$ and $\theta_{13} = 5^\circ$.

θ_{13} and the sparticle spectrum will be a powerful tool for shedding some light on the otherwise unreachable heavy neutrino parameters. Furthermore, in the case of a NUHM scenario, it may also provide interesting information on the Higgs sector. It is clear from this study that the connection between LFV and neutrino physics will play a relevant role for the searches of new physics.

We acknowledge Ana M. Teixeira and Stefan Antusch for their participation in our previous works. M.J. Herrero thanks the organizers for her invitation to this fruitful conference. Financial support from the Spanish MEC, via AP2003-3776 and FPA2006-05423, and from the 'Comunidad de Madrid', via HEPHACOS is also acknowledged.

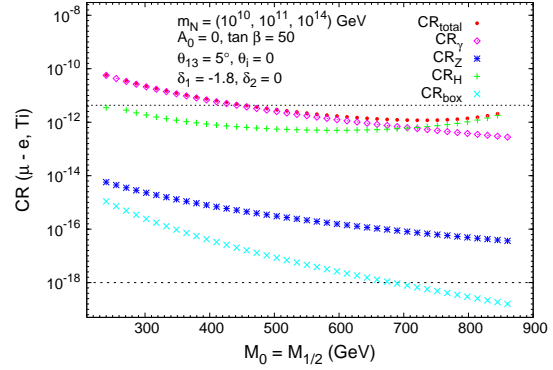


Fig. 7. Contributions to $\text{CR}(\mu - e, \text{Ti})$: total (dots), γ -penguins (diamonds), Z -penguins (asterisks), H -penguins (crosses) and box diagrams (times) as a function of $M_0 (= M_{1/2})$ for the NUHM case with $\delta_1 = -1.8$, $\delta_2 = 0$, $\tan \beta = 50$, $m_{N_i} = (10^{10}, 10^{11}, 10^{14})$ GeV, $\theta_{13} = 5^\circ$ and $R = 1$ ($\theta_i = 0$). The upper (lower) horizontal line denotes the present experimental bound (future sensitivity).

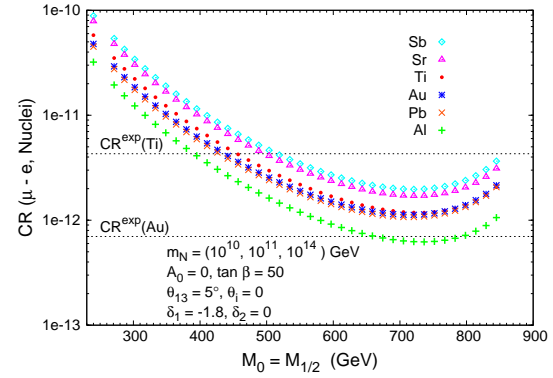


Fig. 8. $\mu - e$ conversion rates as a function of $M_0 = M_{1/2}$ in the NUHM-seesaw for various nuclei: Sb, Sr, Ti, Au, Pb and Al nuclei (diamonds, triangles, dots, asterisks, times and crosses, respectively), with $m_{N_i} = (10^{10}, 10^{11}, 10^{14})$ GeV, $A_0 = 0$, $\tan \beta = 50$, $\theta_{13} = 5^\circ$, $\theta_i = 0$, $\delta_1 = -1.8$ and $\delta_2 = 0$. From top to bottom, the horizontal dashed lines denote the present experimental bounds for $\text{CR}(\mu - e, \text{Ti})$ and $\text{CR}(\mu - e, \text{Au})$.

References

1. J. A. Casas and A. Ibarra, Nucl. Phys. B 618 (2001) 171 [arXiv:hep-ph/0103065].
2. E. Arganda and M. J. Herrero, Phys. Rev. D **73** (2006) 055003 [arXiv:hep-ph/0510405].
3. S. Antusch, E. Arganda, M. J. Herrero and A. M. Teixeira, JHEP **0611** (2006) 090 [arXiv:hep-ph/0607263].
4. E. Arganda, M. J. Herrero and A. M. Teixeira, arXiv:0707.2955 [hep-ph]. To appear in JHEP (2007).
5. B. C. Allanach *et al.*, in *Proc. of the APS/DPF/DPB Summer Study on the Future of Particle Physics (Snowmass 2001)* ed. N. Graf, Eur. Phys. J. C **25** (2002) 113 [eConf C010630 (2001) P125] [arXiv:hep-ph/0202233].